JOURNAL OF GEOPHYSICAL RESEARCH, VOL. 111, D24204, doi:10.1029/2005JD006733, 2006

Implementation of cloud retrievals for Tropospheric Emission Spectrometer (TES) atmospheric retrievals: part 1. Description and characterization of errors on trace gas retrievals

Susan S. Kulawik,[1] John Worden,[1] Annmarie Eldering,[1] Kevin Bowman,[1] Michael Gunson,[1] Gregory B. Osterman,[1] Lin Zhang,[2] Shepard A. Clough,[3] Mark W. Shephard,[3] and Reinhard Beer[1]

Received 3 October 2005; revised 17 February 2006; accepted 16 June 2006; published 22 December 2006.

[1] We develop an approach to estimate and characterize trace gas retrievals in the presence of clouds in high spectral measurements of upwelling radiance in the infrared spectral region (650–2260 cm^{-1}). The radiance contribution of clouds is parameterized in terms of a set of frequency-dependent nonscattering optical depths and a cloud height. These cloud parameters are retrieved jointly with surface temperature, emissivity, atmospheric temperature, and trace gases such as ozone from spectral data. We demonstrate the application of this approach using data from the Tropospheric Emission Spectrometer (TES) and test data simulated with a scattering radiative transfer model. We show the value of this approach in that it results in accurate estimates of errors for trace gas retrievals, and the retrieved values improve over the initial guess for a wide range of cloud conditions. Comparisons are made between TES retrievals of ozone, temperature, and water to model fields from the Global Modeling and Assimilation Office (GMAO), temperature retrievals from the Atmospheric Infrared Sounder (AIRS), tropospheric ozone columns from the Goddard Earth Observing System (GEOS) GEOS-Chem, and ozone retrievals from the Total Ozone Mapping Spectrometer (TOMS). In each of these cases, this cloud retrieval approach does not introduce observable biases into TES retrievals.

Citation: Kulawik, S. S., J. Worden, A. Eldering, K. Bowman, M. Gunson, G. B. Osterman, L. Zhang, S. Clough, M. W. Shephard, and R. Beer (2006), Implementation of cloud retrievals for Tropospheric Emission Spectrometer (TES) atmospheric retrievals: part 1. Description and characterization of errors on trace gas retrievals, *J. Geophys. Res.*, *111*, D24204, doi:10.1029/2005JD006733.

1. Introduction

[2] Infrared remote sensing of the Earth's atmospheric state and composition is challenged by the radiative effects of clouds, which can be computationally demanding if such effects as multiple scattering are to be considered. Traditional approaches for operational sounding systems to retrieve atmospheric temperature, humidity, and trace gases in the lower atmosphere have tried either to search for cloud free scenes by using threshold based algorithms to detect clouds and develop cloud masks [*King et al.*, 1992; *King et al.*, 2003; *Platnick et al.*, 2003; *Ackerman et al.*, 1998; *Menzel et al.*, 1983; *Smith et al.*, 1970] or to use cloud clearing, whereby several adjacent observations are combined to estimate a cloud-free radiance [*Chahine*, 1974; *Chahine*, 1977; *Chahine et al.*, 1977; *Susskind et al.*, 2003]. Both approaches avoid the need for complex modeling of cloud effects but have currently been applied to data sets with dense data coverage (which can compensate for the rejection of difficult cases). They also have the added complexity of characterizing errors resulting from unmodeled cloud fields.

[3] The Tropospheric Emission Spectrometer (TES), on the Earth Observing System Aura (EOS-Aura) platform, obtains high spectral resolution nadir infrared emission measurements (650 cm^{-1}–2260 cm^{-1}, with spectral sampling distance of 0.06 cm^{-1} for nadir viewing mode) at a comparatively low spatial sampling (about 3500 observations every other day) [*Beer*, 2006]. Neither cloud masking nor cloud clearing are possible approaches in these circumstances if a scientifically useful number of retrievals are to be obtained. In this paper we describe a simple single-layer cloud model used in the forward model for TES retrievals. This approach has been tested with simulated observations where the effects of a wide range of cloud conditions were fully modeled to establish the retrieval uncertainties for the radiances and trace gases. Further-

[1] Jet Propulsion Laboratory/California Institute of Technology, Pasadena, California, USA.
[2] Department of Earth and Planetary Sciences, Harvard University, Cambridge, Massachusetts, USA.
[3] Atmospheric and Environmental Research Inc. (AER), Lexington, Massachusetts, USA.

0148-0227/06/2005JD006733$09.00

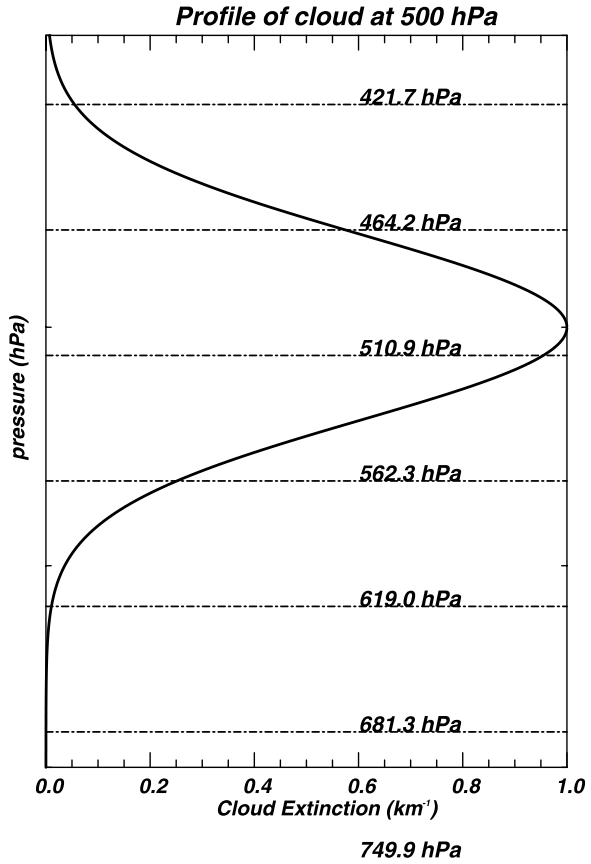

Figure 1. The extinction profile of a cloud at 500 hPa with $\kappa(\nu_c) = 1\ \mathrm{km}^{-1}$. Tropospheric Emission Spectrometer (TES) forward model levels are shown with dashed lines.

more, comparisons with coincident measurements by other satellite instruments as well as model fields are used to establish any potential bias or systematic errors of the approach.

2. Cloud Parameterization and Retrieval Approach

[4] The choice of cloud parameterization was driven by the desire for analytic Jacobians (the derivative of the radiance with respect to cloud parameters), computational tractability, and retrieval stability. This led to the choice of a single-layer cloud and an effective optical depth that is coarsely spaced in wavenumber by 25 to 100 cm^{-1}. The effective optical depth accounts for both cloud absorption and scattering. To ensure analytic Jacobians for the cloud top height, we constrained the cloud to have a Gaussian profile in altitude. Consequently, cloud parameterization can be described as a frequency-dependent layer effective optical depth, τ, for a layer at pressure $\overline{P}_l$:

$$\tau\left(\nu_c, \overline{P}_l\right) = \kappa(\nu_c) e^{-\beta\left(\ln \overline{P}_l - \ln P_c\right)^2} \Delta s \tag{1}$$

where κ is the frequency-dependent layer average effective extinction coefficient, β is the Gaussian width parameter, P_c is the cloud altitude (note that this is not frequency dependent) and Δs is the layer thickness. An example of the cloud is shown in Figure 1. Note that log (κ_ν) and log (P_c) are the retrieved parameters.

[5] The cloud optical depth shown in equation (1) is defined on a coarse frequency grid ν_c (spaced by 25 or 100 cm^{-1}) and is linearly interpolated to the TES unconvolved (before the instrument line shape) frequency grid ν_{mono} (0.0002–0.0008 cm^{-1} spacing) using the following equations:

$$\tau\left(\nu_{mono}, \overline{P}\right) = (1-\alpha)\tau\left(\nu_l, \overline{P}\right) + \alpha\tau\left(\nu_{l+1}, \overline{P}\right) \tag{2}$$

$$\alpha = \frac{\nu_{mono} - \nu_l}{\nu_{l+1} - \nu_l} \text{ when } \left(\nu_l \le \nu_{mono} \le \nu_{l+1}\right) \tag{3}$$

[6] Once the cloud optical depth is computed for a layer on the monochromatic grid, it is added to the total optical depth for each layer.

$$\boldsymbol{\tau}_{total} = \boldsymbol{\tau}_{gas} + \boldsymbol{\tau}_c \tag{4}$$

[7] The radiative transfer calculates the observed radiance on the basis of the total optical depth for each layer, as discussed below in section 2.2. The radiance is then interpolated (to speed up calculations) to the TES convolved grid ($\boldsymbol{\nu}_{\mathrm{conv}} = 0.06\ \mathrm{cm}^{-1}$ spacing for nadir), convolved with the TES instrument line shape, and apodized [*Norton and Beer*, 1976]. For more details on the TES radiative transfer, see *Clough et al.* [2006].

2.1. Radiative Transfer With and Without Scattering Clouds

[8] The algorithmic approach uses nonscattering clouds to reduce algorithm complexity and processing time. This section compares the algorithm used to compute radiation from scattering clouds versus the algorithm used to compute radiation from nonscattering clouds in order to see how the nonscattering assumption affects calculated radiances. For scattering clouds, the radiation reaching the top of the atmosphere ($\boldsymbol{I_{TOA}}$) can be expressed by the following equation [*Wei et al.*, 2004]:

$$I_{TOA} = I_1^{\uparrow} T_c T_3 + (1 - R_c - T_c) B_c T_3 + I_3^{\uparrow} + I_3^{\downarrow} R_c T_3 \tag{5}$$

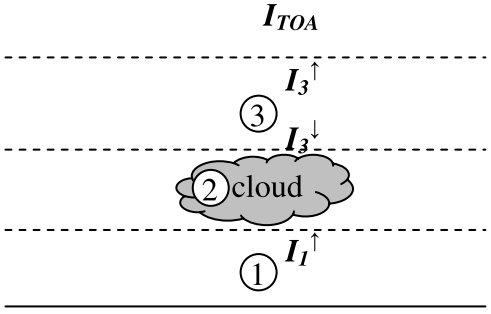

Figure 2. Diagram of radiative transfer through a homogeneous one-layer cloud. Regions 1 and 3 are cloud-free, and region 2 contains a cloud. The various $\boldsymbol{I}$'s represent radiation entering or leaving the different regions.

Table 1. Cloud-Effective Extinction Initial Guess and A Priori Value ("Cloud-Effective Extinction") Set by the Brightness Temperature (BT) Difference

BT Range (K)	Cloud-Effective Extinction
>20	4
10–20	1.3
6–10	0.8
0–6	0.015

where (see Figure 2):

$I_1^{\uparrow}$ is the atmospheric radiation reaching the cloud's lower boundary

T is transmittance: T_c is cloud transmittance, T_3 is the transmittance above the cloud.

R_c is the cloud reflectance

B_c is the blackbody radiation at the cloud temperature

$I_3^{\uparrow}$ is the upward emission from above the cloud that reaches the top of the atmosphere

$I_3\downarrow$ is the downward emission from above the cloud that reaches the cloud's upper boundary.

[9] For a nonscattering cloud the radiation field at the top of the same atmosphere is

$$I_{TOA} = I_1^{\uparrow} T_c' T_3 + \left(1 - T_c'\right) B_c T_3 + I_3^{\uparrow} \tag{6}$$

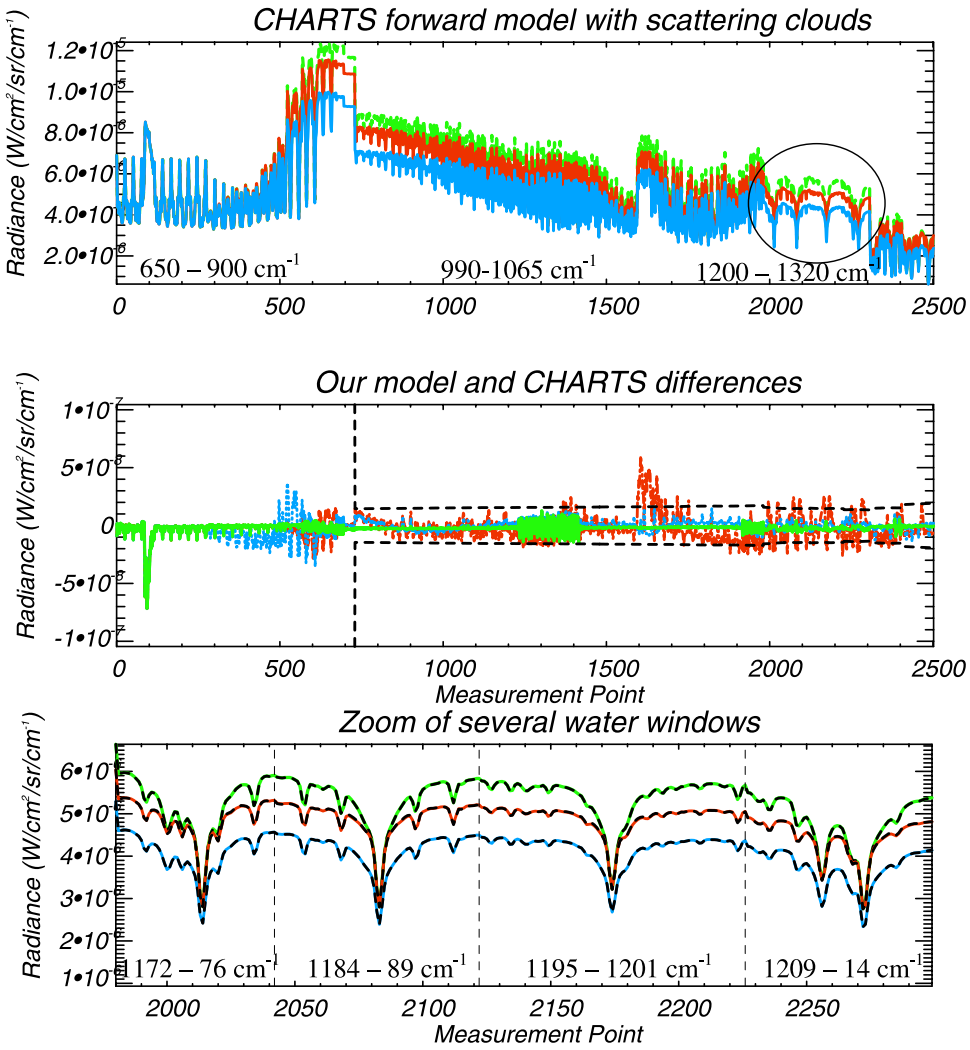

Figure 3. Comparison of CHARTS and our nonscattering forward model simulated radiances, where CHARTS includes scattering while ours does not. (top) Radiance values from CHARTS over the 2500 measurement points (out of the 18,000+ total TES measurement points) used for TES retrieval of a cloud-free scene (green), an ice cloud at 300 mb (blue), and a water cloud at 715 mb (red). (middle) Difference between CHARTS and our nonscattering forward model with the dashed line showing measurement error for the TES instrument. (bottom) A zoom-in of the oval in Figure 3, top, showing four windows (denoted by dashed lines) is in the water region (1172–1214 cm^{-1}) with our nonscattering model plotted as the black dashed line. Both models accurately capture large and small features for different cloud conditions, with low clouds showing the greatest differences.

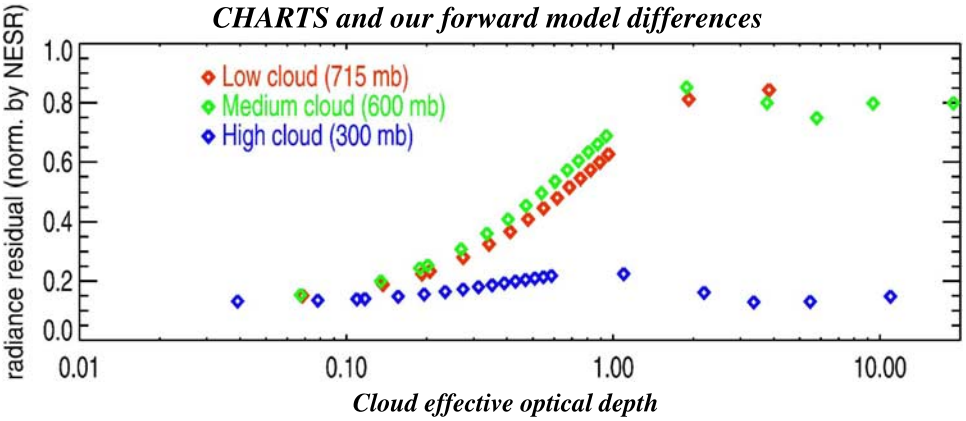

Figure 4. Average radiance residual RMS between CHARTS and our nonscattering forward model simulated radiances normalized by the measurement error for the TES instrument for a range of cloud cases. This shows that the error resulting from our cloud parameterization is less than the measurement error for the TES instrument for all cloud cases.

[10] Equation (6) is equation (5) with R_c set to 0. The two equations describe the same radiation field if T'_c (our effective transmittance) is

$$T'_c = T_c - R_c \frac{I_3^{\downarrow} - B_c}{I_1^{\uparrow} - B_c} \tag{7}$$

[11] Equation (6), the nonscattering description, is adequate when the second term of equation (7) is small and/or is a slowly varying function of frequency. Since $I_3^{\downarrow}$ and $I_1^{\uparrow}$ vary rapidly with frequency, this condition is only met when $R_c \ll T_c$ and/or the standard deviation of $\left(\frac{I_3^{\downarrow}-B_c}{I_1^{\uparrow}-B_c}\right)$ is much less than its mean. Studies with simulated data in section 3.1 show that the limit is achieved over the thermal infrared and that the residual high-frequency error is less than the NESR of data taken by the TES instrument.

2.2. Broken Clouds

[12] This approach accounts for both uniform and broken cloud scenes. A broken cloud is mathematically identical to a uniform, less optically thick cloud, if the atmosphere is otherwise homogeneous (Appendix A). The result shown in Appendix A demonstrates that radiance observed from broken cloud scenes are equivalent to those with a homogeneous, thinner cloud. However, this approach only works for a homogenous or broken layer of single-layer clouds and does address double-layer clouds.

2.3. TES Cloud Retrieval Strategy

[13] Cloud parameters are jointly retrieved with surface temperature, emissivity, atmospheric temperature, water, and ozone using the TES nonlinear optimal estimation algorithm [*Bowman et al.*, 2006; *Bowman et al.*, 2002; *Worden et al.*, 2004]. As with other atmospheric parameters, an optimal estimate of these parameters requires an initial guess profile, an a priori profile, and a constraint matrix, as well as the ability to calculate Jacobians (derivatives of TES radiance with respect to each retrieval parameter). This approach allows trace gases and temperature profiles to be retrieved in the presence of clouds, and allows the characterization of trace gas errors and sensitivities in the presence of clouds.

[14] The implementation of this approach requires a strategy, including determination of the cloud initial guess, possible initial guess refinements, and the creation of a realistic a priori covariance and constraint to regularize cloud retrievals. A good retrieval strategy is necessary to mitigate the nonlinear effects of clouds on the retrieval. Another key component to the retrieval strategy is the decision to retrieve cloud extinction and cloud pressure in log. This allows the cloud extinction to vary over orders of magnitude in the retrieval process, and also passively constrains the cloud extinction to be positive.

[15] The cloud-effective extinction initial guess and a priori are set using the average brightness temperature in the 11 μm atmospheric window region (867.04–900 cm^{-1}). The initial guess and a priori are set, as shown in Table 1, from the difference between the observed radiance and simulated brightness temperature in the window region using a cloud-free initial guess based on GMAO temperature and water. The initial guess and a priori for cloud pressure are always set to 500 mb. If the brightness temperature difference in the 11 μm region is greater than 6K, a refinement step is inserted into the retrieval process. In the refinement step, only the cloud-effective extinctions and cloud pressure parameters are retrieved with the rest of the atmosphere fixed to the initial guess. The initial guess refinement for the clouds is similar to the initial guess update (shape retrieval) that has been done for ozone retrievals [*Clough et al.*, 2002]. Following this possible step, cloud parameters are retrieved in every step along with the atmospheric parameters of interest.

[16] The covariance of the cloud-effective extinction parameters was created with the assumption that the cloud's effective extinction varies significantly from target to target, and the cloud optical depth is highly correlated over all frequencies. For the first assumption, the diagonal elements were set to 10 for the covariance of the log of the effective cloud extinction. For the second assumption, all off-diagonal elements were set to 0.9 * diagonal. The covariance of logarithm of the cloud pressure is set to 1, which has

Table 2. TES Sensitivity to Ozone Below a Cloud for Actual Data From a TES Step and Stare From 21 September 2004[a]

Cloud O.D.(<500 mb)	DOF (>500 mb)	TES Sensitivity
0	~0.8	100%
0.1	~0.5	~60%
1.0	~0.25	~30%

[a]The sensitivity drop off is approximate because the sensitivity depends on other factors, such as atmospheric temperature, ozone concentration, and surface conditions, which also change from target to target.

1-sigma range of about 183 mb–1300 mb. This covariance was used as the a priori error in equation (13). The inverse of the covariance is used as the constraint for cloud-effective extinction.

2.4. Error Analysis

[17] An advantage of the integration of the cloud parameters into the forward model and retrievals is that the error analysis for these can be handled with the same equations and methodology as the error analysis for all other atmospheric retrieved parameters. The error analysis used is described in detail by *Bowman et al.* [2006], *Worden et al.* [2004], and more generally by *Rodgers* [2000].

2.4.1. Linear Estimate for Simulated Data

[18] If the estimated state calculated from the nonlinear least square algorithm is "close" to the actual state, then the estimated state can be expressed in terms of the actual state through the linear retrieval [*Bowman et al.*, 2006; *Rodgers*, 2000]:

$$\mathbf{x}_{est} = \mathbf{x}_a + \underbrace{\mathbf{A}(\mathbf{x}_{true} - \mathbf{x}_a)}_{\text{smoothing}} + \underbrace{\mathbf{G}\mathbf{n} + \mathbf{G}\mathbf{K}_b}_{\text{measurement}} \underbrace{(\mathbf{b}_{true} - \mathbf{b}_{est})}_{\text{systematic}} \quad (8)$$

where $\mathbf{x}_{est}$ is the retrieved state expressed as an N element real vector, $\mathbf{A}$ is the averaging kernel matrix, $\mathbf{n}$ is the noise vector, $\mathbf{x}_{true}$ is the "true" atmospheric state vector, $\mathbf{x}_a$ is the a priori state vector, $\mathbf{b}$ is a vector composed of nonretrieved atmospheric parameters, $\mathbf{b}_{est}$ is composed of the values used in the forward model for those nonretrieved parameters, $\mathbf{G}$ is the gain matrix, which is defined by

$$\mathbf{G} = \frac{d\mathbf{x}}{d(\mathbf{radiance})} = \left(\mathbf{K}^T\mathbf{S}_m\mathbf{K} + \Lambda\right)^{-1}\mathbf{K}^T\mathbf{S}_m^{-1}, \quad (9)$$

where

$$\mathbf{S}_m = \langle \mathrm{n}\mathrm{n}^T \rangle$$

is the measurement error covariance matrix, and $\mathbf{\Lambda}$ is the constraint. The Jacobian, $\mathbf{K}$, is defined by

$$\mathbf{K} = \frac{\partial \mathbf{L}}{\partial \mathbf{x}} \quad (10)$$

where $\mathbf{L}$ is the radiance, and $\mathbf{K}_b$ is the Jacobian defined with respect to $\mathbf{b}$. Equation (8) is a valid approximation to the nonlinear retrieval when

$$\mathbf{K}(\mathbf{x}_{true} - \mathbf{x}_{est}) \approx \mathbf{L}(\mathbf{x}_{true}, \mathbf{b}) - \mathbf{L}(\mathbf{x}_{est}, \mathbf{b}). \quad (11)$$

[19] The averaging kernel matrix, $\mathbf{A} = \partial \mathbf{x}_{true}/\partial \mathbf{x}_{est}$, is the sensitivity of the retrieval to the true state of the atmosphere and is computed as

$$\mathbf{A} = \frac{\partial \mathbf{x}_{true}}{\partial \mathbf{x}_{est}} = \frac{\partial \mathbf{x}_{true}}{\partial \mathbf{L}} \frac{\partial \mathbf{L}}{\partial \mathbf{x}_{est}} = \mathbf{G}\mathbf{K}. \quad (12)$$

[20] Equation (8) is composed of three terms that are sources of error in a retrieval. The first term involving the

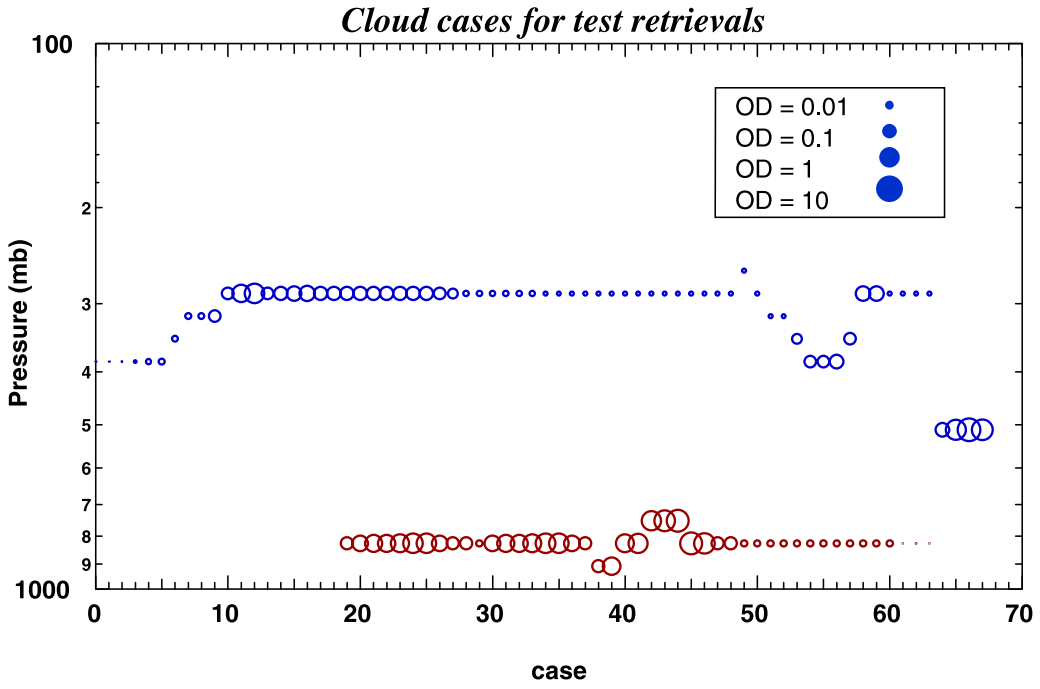

Figure 5. Cloud cases used to test retrievals in the presence of clouds. Red and blue dot sizes show the optical depths (which range from 0.002 to 6.5) of high-ice and low-water clouds, respectively, for each case. Cases include low-water clouds only, high-ice clouds only, double-layer clouds, and no clouds.

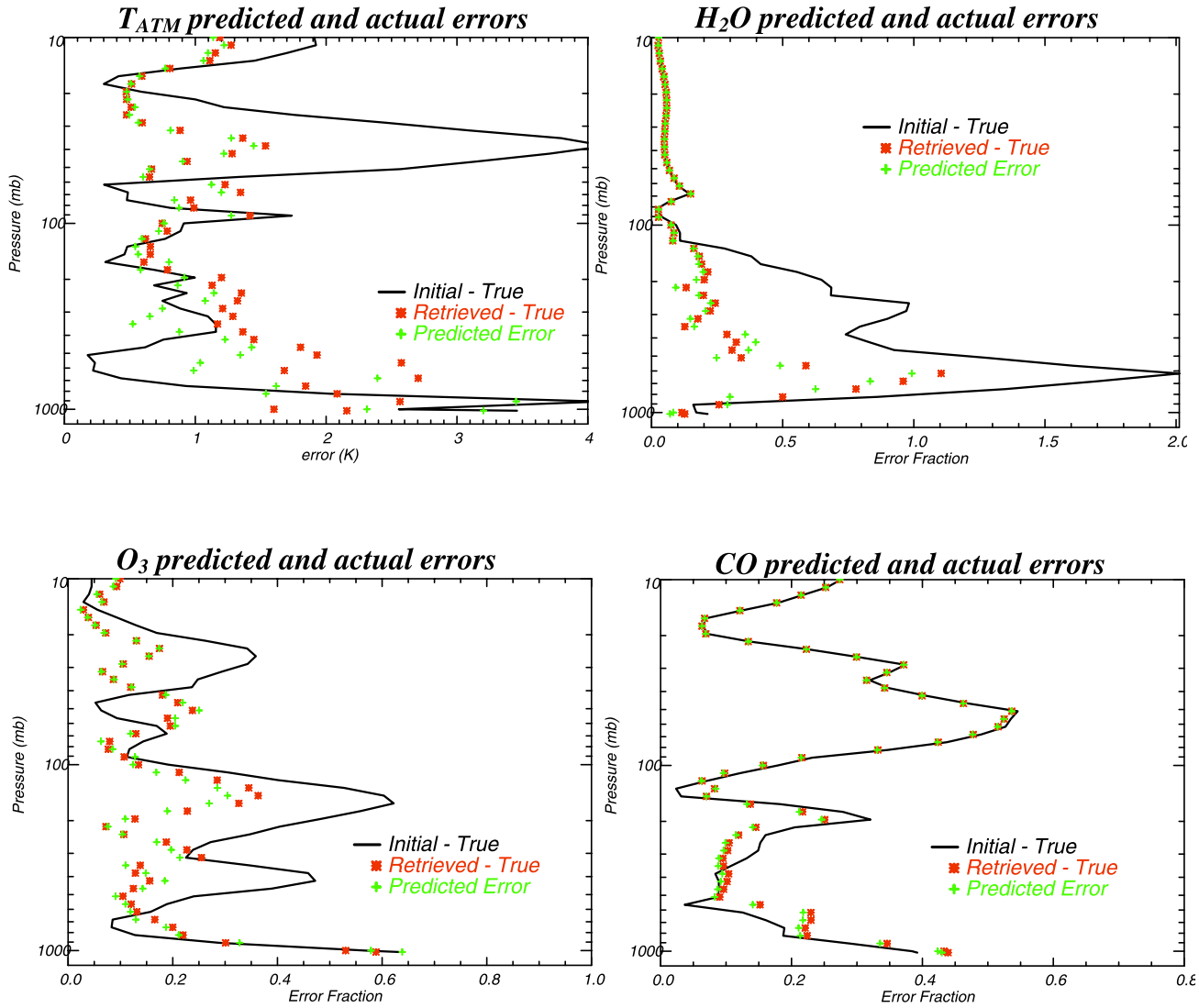

Figure 6. Predicted versus actual errors for ozone, temperature, water, and carbon monoxide for simulated data. Initial error, $\sqrt{\text{covariance}(initial - true)_{ii}}$, is shown in black. Actual error, $\sqrt{\text{covariance}(retrieved - true)_{ii}}$, is shown in red, and the predicted error, $\sqrt{\text{covariance}(x_{est} - true)_{ii}}$ using equation (13), is shown in green. Agreement between the predicted error (equation (13)) and the actual error validates the error analysis. For the retrieved atmospheric gases, error fraction is the error in the logarithm of the VMR, where error fraction = 0.1 corresponds to a 10% error in the VMR.

averaging kernel is the basis for the "smoothing" error, which is due to the unresolved fine structure in the true state and other smoothing effects introduced by the constraint. The second term propagates the effect of random spectral noise into the estimate and the third term quantifies the impact of nonretrieved parameters on the retrieval.

[21] The $\mathbf{x}_{est}$ calculated with equation (8) can be used to compare to the nonlinear retrieval result to check the accuracy of the linear estimate, on which the error analysis shown in equation (13) is based. This comparison is done in section 3.2.

[22] The error covariance can be calculated using equation (8) over an ensemble of cases. The error covariance is defined from the second-order statistics of the difference between retrieved state and the true state:

$$\mathbf{S}_{err} = \left\langle (\mathbf{x}_{est} - \mathbf{x}_{true})(\mathbf{x}_{est} - \mathbf{x}_{true})^T \right\rangle$$

Substituting equation (8) into the above equation and assuming that the atmospheric state, spectral noise, and nonretrieved parameters are uncorrelated result in

$$\mathbf{S}_{err} = \underbrace{(\mathbf{I} - \mathbf{A})\mathbf{S}_a(\mathbf{I} - \mathbf{A})^T}_{\text{smoothing}} + \underbrace{\mathbf{G}\mathbf{S}_m\mathbf{G}^T}_{\text{measurement}} + \underbrace{\mathbf{G}\mathbf{K}_b\mathbf{S}\mathbf{b}_{err}(\mathbf{G}\mathbf{K})^T}_{\text{systematic}} \quad (13)$$

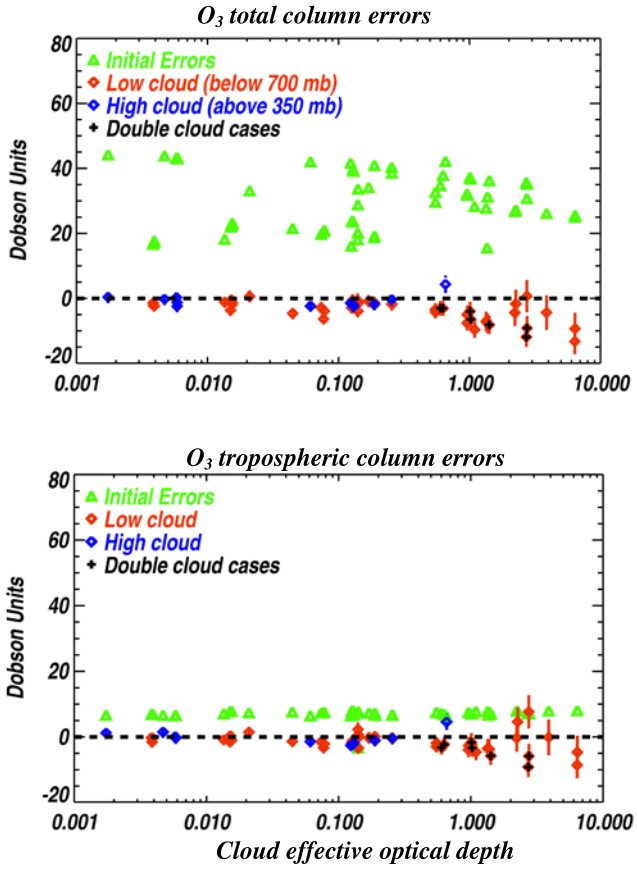

Figure 7. (bottom) Tropospheric and (top) total column results for simulated ozone retrievals in the presence of clouds. Green shows the initial error, (initial − true), red and blue show the actual retrieved error, (retrieved − true) for low and high clouds, respectively, and reported errors (using equation (15)) are shown as error bars. Note that the error bars increase as the actual error increases. The double-layer cloud cases are denoted by (+) and in general have larger errors that are somewhat underreported.

where $\mathbf{S}_a$ is the a priori covariance, $\mathbf{S}_m$ is the measurement error covariance, and $\mathbf{Sb}_{err}$ is the error covariance of systematic error sources. In simulations, the covariance of $(\mathbf{x}_{est} - \mathbf{x}_{true})$ using equation (8) can give a more accurate test of the error analysis than equation (13) because $\mathbf{S}_a$ and $\mathbf{Sb}_{err}$ are frequently inaccurate.

2.4.2. Column Error

[23] A column is the integrated total molecules per cm^2 over all or part of the vertical profile. Column results are useful for intercomparisons because smoothing errors tend to balance out, resulting in column errors far less than error estimates for any given level. This section describes how errors are calculated for a column result.

[24] The column error can be calculated by using the predicted error covariance and the linearized relationship between the column and the profile, which is the first derivative of the column with respect to a gas's volume-mixing ratio (VMR):

$$\frac{d(column)}{dVMR_{est}} = d_c \tag{14}$$

[25] Since trace gases are usually retrieved as the logarithm of the volume-mixing ratio, the error covariance must be converted to a linear error covariance, which is approximately done by multiplying by the volume-mixing ratio (VMR).

[26] The column error covariance is

$$S_{column} = \sum_{i,j} VMR(i) d_c(i) S_{err}(i,j) d_c(j) VMR(j) \tag{15}$$

[27] The square root of the covariance is the predicted column error. Column results and error estimates are shown for simulated data and TES data in the following section. The predicted errors are shown to be accurate and reflect the increasing uncertainty with thicker clouds in section 3.2 (Figure 7).

3. Tests of Assumptions

[28] The following sections show results of our implantation of clouds and cloud retrievals. Results demonstrate that the errors due to our modeling of clouds into the forward model are contained to acceptable levels, that

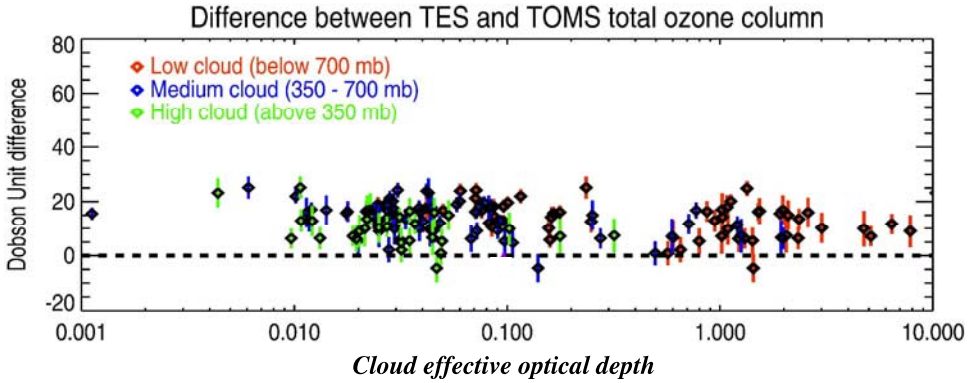

Figure 8. Difference between TES and TOMS results for total ozone column for a TES special observation transect near Ascension Island on 21 September 2004. Although there is a bias with respect to TOMS, there is no apparent dependence on cloud optical depth or height. Reported errors (using equation (15)) are shown as error bars.

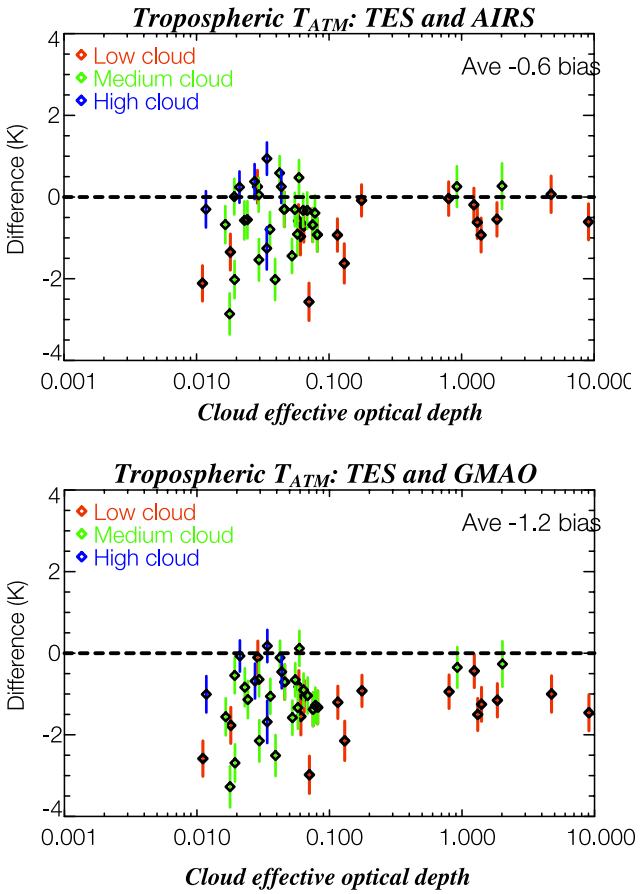

Figure 9. Comparison of average TES Tropospheric temperature to GMAO and AIRS versus retrieved cloud properties. (bottom) TES − GMAO comparison (which is used for the TES a priori) shows an average 1.2K bias with respect to GMAO. However, this bias does not show any trends with cloud height and optical depth. The TES- AIRS comparison show less average bias (0.6K) and also does not show an apparent trend with cloud height or optical depth. Reported errors (using equation (15)) are shown as error bars.

simulated retrievals of atmospheric parameters in the presence of clouds are well characterized, and that comparisons of preliminary TES retrievals to GMAO, AIRS, and TOMS data do not show biases with respect to retrieved cloud-effective optical depth or cloud height. Additionally, results from the TES instrument are shown, which show retrievals of atmospheric ozone and water through a large variety of cloud conditions. The drop-off of degrees of freedom for ozone and water below clouds of various optical depths is also shown.

3.1. Forward Model Errors

[29] To determine the forward model errors, simulated radiances with the cloud parameterization described in section 2 were compared with the Code for High-Resolution Accelerated Radiative Transfer (CHARTS) model [*Moncet and Clough*, 1997], which includes scattering. The atmosphere was fixed to a single tropical atmosphere with 68 different cloud cases, having high (~300 hPa), medium (~590 hPa), or low (~715 hPa) clouds with optical depths between 0 and 20. The cloud parameters were retrieved with all other atmospheric parameters set to their true values (the same values which were used to simulate the data in CHARTS). The cloud parameter retrieval finds the optimal match of the effective extinction to the true extinction with scattering, as described in equation (7). The resulting radiance residuals indicate the forward model errors that result from our cloud parameterization. Both radiative transfers were calculated without the addition of noise.

[30] As an example, Figure 3 shows that this cloud parameterization captures the effects of moderately thick (0.5 OD) low-water cloud or high-ice cloud on the observed thermal infrared radiation field at the top of the atmosphere. Figure 3 (bottom) shows simulated radiances for a set of water lines between 1170–1215 cm^{-1}. The low-water cloud or high-ice cloud have marked effects on both the radiance at the lines and the radiance between lines. These effects are captured both by CHARTS, which includes scattering, and with our nonscattering approach.

[31] Figure 4 shows the resulting average radiance error for all cloud cases, normalized by the measurement error of the TES instrument calculated for the 2500 measurement points used for TES retrievals (between 650 cm^{-1} and 1320 cm^{-1}). Figure 4 shows that high clouds have less radiance error than low and medium clouds. This is probably due to lower downwelling radiance above the clouds and lower emissions from the clouds, making the second (error) term in equation (7) close to zero. Figure 4 also shows the radiance errors flatten out above optical depths of 2. The trend shown in Table 2 indicates that clouds of optical depth 2 should be about opaque, thus thickening the cloud further should not significantly affect radiance errors.

[32] Figure 4 shows that the average radiance error for all cloud cases is less than one, meaning that the effects of clouds of all heights and optical depths on the observed thermal infrared radiation field are modeled by our approach to within the TES instrument error.

3.2. Simulated Retrievals of Trace Gases in Presence of Clouds

[33] Retrievals of temperature and trace gases were calculated using simulated CHARTS radiances which included scattering clouds. These studies determine if the predicted errors for trace gas retrievals are accurate in the presence of clouds for simulated data, and if improvements over the initial guess are possible in the presence of clouds.

[34] For these studies, a second set of simulated radiances was created consisting of 68 different tropical atmospheres and cloud cases. The simulated observed radiances were created using CHARTS with noise added at expected levels for the TES instrument [see *Worden et. al*, 2004]. The cloud content of the cases consists of no clouds, single-layer low-water clouds, single-layer high-ice clouds, and double-layer water/ice clouds (see Figure 5). Each target is retrieved with the retrieval process outlined in section 2.3 to determine the cloud initial guess, followed by a temperature/water joint retrieval (with clouds), and an ozone retrieval (with clouds).

[35] Figures 6a–6c shows that the retrieval strategy and algorithms described in this paper results in an improvement over the initial guess for temperature, water, and ozone, and that the predicted errors match the actual errors in the

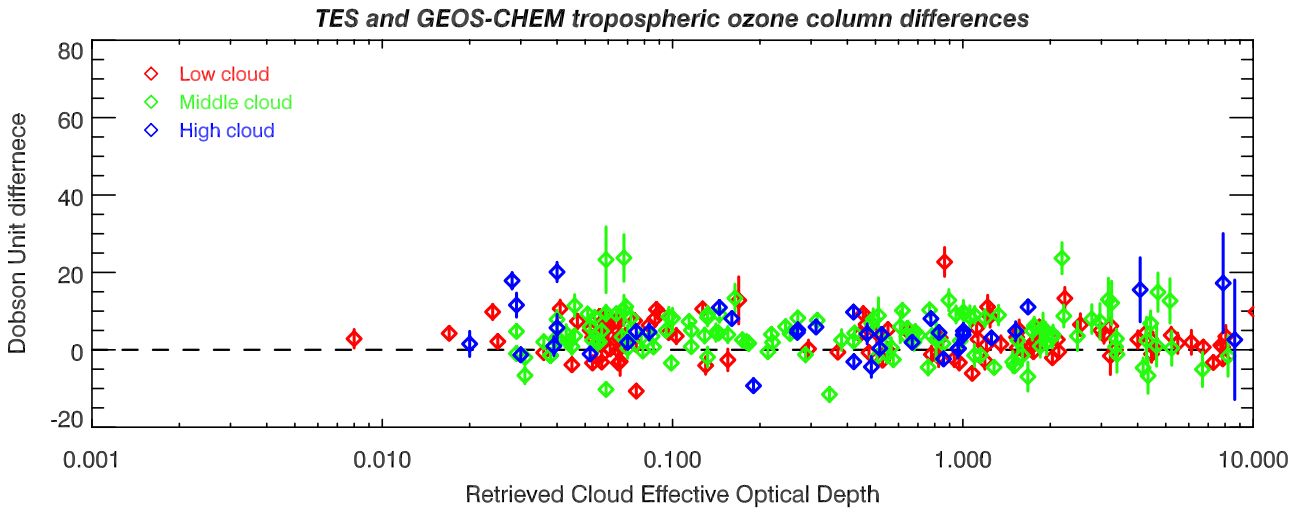

Figure 10. Differences between TES results and the GEOS-Chem model for tropospheric ozone column from a global survey taken on 21 September 2004. Although there is a bias between the TES result and the GEOS-Chem model, there is no apparent dependence on cloud optical depth or height. Error bars are TES-reported tropospheric ozone column error values, since there is no error value reported in the GEOS-Chem model output.

presence of clouds. These figures show the initial error, (from the calculated covariance of initial versus true), the predicted error (using equation (8)), and the actual error (from the calculated covariance of retrieved versus true), all averaged over the ensemble of cases. These plots show that reported errors in the presence of clouds are expected to be accurate (assuming that the a priori covariances are correct) for ozone, water, and temperature above 500 mb, and that improvements over the initial atmospheric guess are achieved even in the presence of clouds.

[36] Figure 7 shows results for tropospheric and total ozone columns versus cloud optical depth and cloud height. The column initial error, retrieved error, and predicted error (using equation (13)) are shown versus cloud optical depth and height, showing that the retrieved columns show little or no bias with cloud height and optical depth for the simulated data set, and that the reported errors increase appropriately with actual error. This shows a lack of bias in retrievals with respect to retrieved cloud properties, and that the reported errors are accurate.

3.3. Results Using Data From the TES Instrument

[37] We demonstrate retrievals in the presence of clouds using "Step and Stare" observations from the TES instrument. "Step and Stare" observations consist of 150 nadir observations spaced approximately 0.4 degrees apart (shown in Figure 11, section 3.3.2) with each target covering a 5 × 8 km footprint. The TES retrieval results reported in this paper are from v001 data and are considered to be of beta quality. TES data and documentation, such as the "Level 2 Data User's Guide," are available from the Langley Atmospheric Data Center athttp://eosweb.larc.nasa.gov/PRODOCS/tes/table_tes.html.

3.3.1. Comparisons of TES to TOMS, GMAO, GEOS-Chem and AIRS in the Presence of Clouds

[38] We compare TES results for a Step and Stare that ranges from −32° S to 32° N near Ascension Island (7.917° S, 14.417° W) on 21 September 2004 to (1) TOMS total ozone column [*McPeters et al.*, 1998], (2) GMAO tropospheric temperature [*Bloom et al.*, 2005], and (3) AIRS tropospheric temperature [*Aumann et al.*, 2003]. We also compare TES results from a global survey to the GEOS-Chem model [*Bey et al.*, 2001] for tropospheric ozone column.

[39] Differences between TES and TOMS total ozone columns are compared to the retrieved cloud optical depth and retrieved cloud height in Figure 8. This comparison shows that although there is a bias with respect to TOMS, there is no apparent dependence on cloud optical depth or height.

[40] For the TES versus AIRS comparisons we found a total of 47 temperature and water retrievals from TES and AIRS that were both colocated and were of good quality based on the AIRS data quality flags. For example, only AIRS cases with a quality flag of 0 or 10 were chosen. We first compute an average retrieved temperature in the troposphere (from the surface to 100 mb). The difference between the average retrieved temperature from TES and AIRS for these retrievals is compared to the retrieved cloud optical depth and retrieved cloud height in Figure 9, top. While there is an apparent bias of 0.6K, it is not dependent on the retrieved cloud optical depth or height. Note that TES and AIRS are presently using two difference spectral regions for temperature retrievals with TES using the ozone band and water regions around 1200 cm^{-1} and AIRS using the co2 $\nu 2$ region. TES temperature retrievals are presently being evaluated by the TES science team [*Shephard et al.*, 2005].

[41] A similar comparison is shown between TES tropospheric temperature and GMAO tropospheric temperature for the same 47 cases in Figure 9, bottom. The GMAO temperature fields are linearly interpolated to the TES latitude, longitude, and time and an average tropospheric temperature for these fields is calculated. Although TES retrievals use GMAO fields for the a priori and initial guess, the temperature residuals between TES and GMAO show a

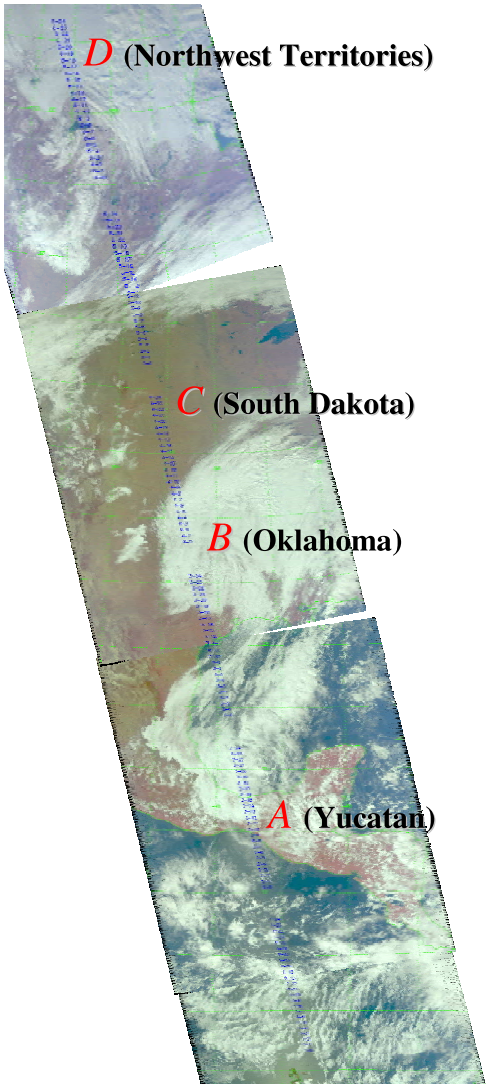

Figure 11. TES "Step and Stare" for 3 November 2004. The TES observation locations (shown in blue) are superimposed onto an AIRS-visible image. A large variety of cloud cases are seen in this special observation: scattered (A), storm system (B), clear (C) and clear with icy groundcover (D).

relatively consistent bias of 1.2K with respect to GMAO, but no apparent bias with respect to cloud optical depth or height. Comparisons between TES and GMAO tropospheric water were similarly done, and no apparent bias with respect to cloud optical depth or height was seen.

[42] Comparisons are shown between TES tropospheric ozone columns and results from the Goddard Earth Observing System (GEOS) Chem model. Data was generated by the GEOS-Chem model v7.01.02 driven by GEOS assimilated meteorological observations from the NASA Global Modeling and Assimilation Office (GMAO) [*Bey et al.*, 2001]. Comparisons were made by matching Near-Real-Time (NRT) simulations from the GEOS-Chem model (http://coco.atmos.washington.edu/cgi-bin/ion-p?page = geos_nrt.ion) at the same observation time and locations as TES observations between 40S and 40N latitudes for a TES Global Survey taken on 21 September 2004. GEOS-Chem simulated ozone profiles at TES observation locations were processed through TES averaging kernels [*Rodgers*, 2000]. GEOS-Chem tropospheric ozone columns are obtained from integrating model profiles up to the TES-defined tropopause. Figure 10 shows the difference between GEOS-Chem tropospheric ozone column and the TES retrieved tropospheric ozone column versus cloud optical depth and height. Although a bias is seen with respect to GEOS-Chem, there is no apparent dependence on the retrieved cloud parameters.

3.3.2. TES Ozone and Water Profile Results in the Presence of Clouds

[43] Figure 11 shows the cloud and surface conditions observed by a TES "Step and Stare" taken on 3 November 2004 ranging from 1° north to 65° north, passing near Houston, Texas (29.77° N, −95.39° W). The observation locations are shown, in blue, superimposed on an AIRS-visible image, which show cloud locations and cloud conditions. The retrieval results for ozone and water for these targets is shown in Figure 12, with the retrieved cloud-effective optical depths represented by the size of the grey circle placed at the retrieved cloud pressure. The retrievals from TES data suggest a stratospheric intrusion event at 35° north, with increased tropospheric ozone and corresponding decreased upper-tropospheric water. These variations correspond with the storm system at approximately 34° north seen in Figure 11. The retrieved profiles show spatial variations that are apparently independently of clouds, such as the tropopause height drop with latitude indicated by the ozone and water profiles between 45° and 55°, variations in the water abundances surrounding the storm system at about 34° north, and the stratospheric intrusion seen at around 35° north.

3.4. Sensitivity to Ozone Below Clouds of Various Optical Depths

[44] Characterization of retrievals of atmospheric species in the presence of clouds is an important consequence of the implementation of the cloud retrieval described in this paper. Sensitivity of retrievals from TES data to lower-tropospheric abundances of ozone was calculated for data containing retrieved clouds of varying optical depths using the Step and Stare described in section 3.3.1. Sensitivity was determined by calculating the degrees of freedom, which is defined as $\sum \text{Ave\_kernel}_{ii}$ below 500 mb. Table 2 shows the attenuation of the lower-tropospheric ozone signal below clouds of various optical depths, showing that about 30% of the sensitivity remains (relative to clear-sky) below an effective O.D. 1.0 cloud. This dropoff is approximate because the sensitivity, in addition to the cloud conditions, depends on atmospheric temperature, surface temperature, and ozone concentrations, which vary from target to target. Below thick clouds, the decreased sensitivity means that results tend to stay at the a priori value (or at the a priori slope, if a first derivative Tikhonov constraint is used).

3.5. Summary and Conclusions

[45] We demonstrate temperature and trace gas retrievals in the presence of clouds which are implemented in the forward model as a single-layer Gaussian vertical profile

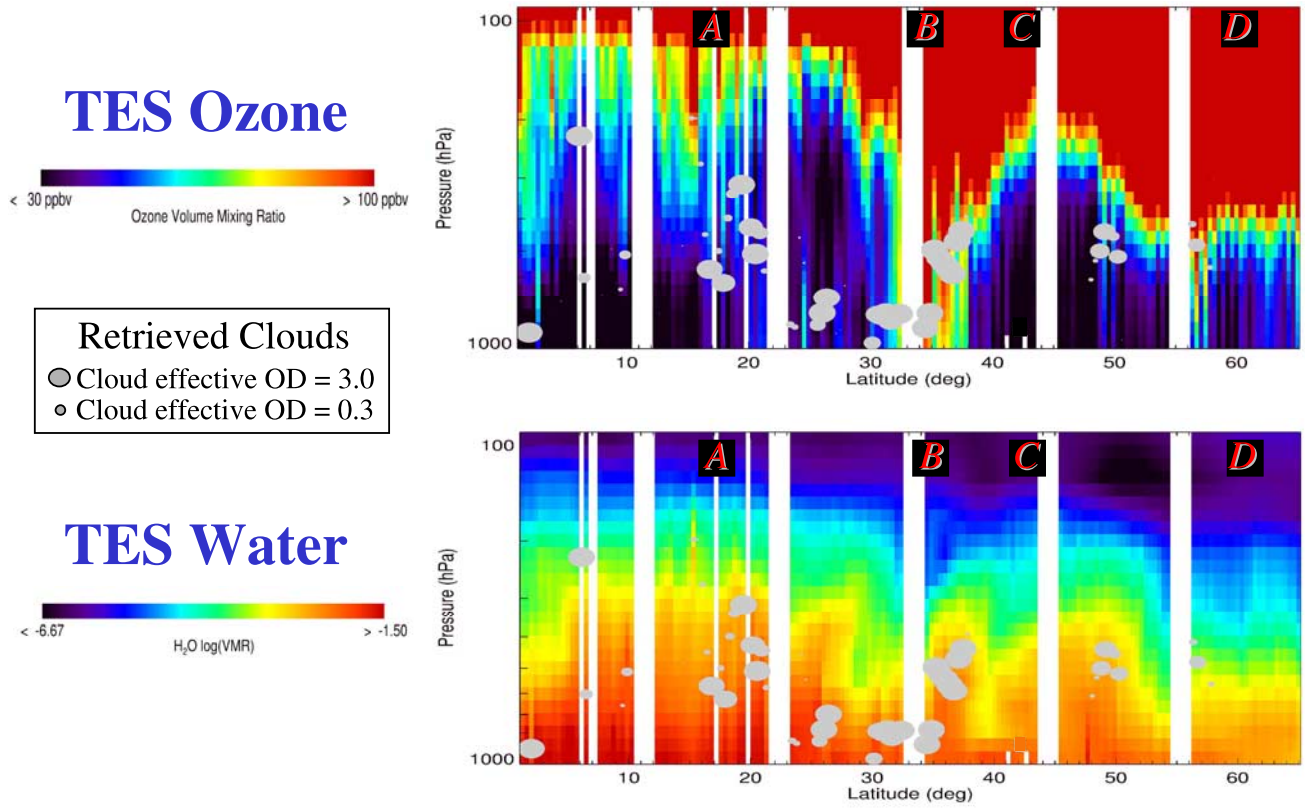

Figure 12. Results from the special observation (11/3/04) shown in Figure 11. Results for ozone and water are shown as curtain plots, with pressure on the y axis, latitude on the x axis, and color representing volume-mixing ratio. Clouds are shown as gray circles with the cloud pressure represented by the circle location and cloud optical depth represented by the circle size. The labels A, B, C, and D correspond to the locations shown in Figure 11.

parameterized by a cloud height and a set of frequency-dependent effective (nonscattering) optical depths. Comparison of this forward model to a full-scattering forward model demonstrates that errors introduced by this cloud parameterization are within the measurement error seen by the TES instrument. Retrievals from data simulated using a full-scattering forward model show our retrieval approach improves over the initial guess in the presence of clouds (i.e., adds to the knowledge of atmospheric abundances). Error estimates for atmospheric abundances are verified using simulated data, and show increasing uncertainties as cloud optical depths increase. Comparisons between retrieval results from the TES instrument and GMAO, GEOS-Chem, AIRS, and TOMS fields for temperature, water, and ozone show no apparent biases with respect to the retrieved cloud optical depth or cloud pressure. Results shown for TES observations of ozone and water through a variety of cloudy conditions taken on 4 November 2004 show spatial variations that correlate with a visible storm system and vary as expected with latitude and altitude. Use of this algorithm and approach to model clouds is allowing data from the TES instrument to be processed through a large range of cloud conditions and produce near-global, unbiased with respect to cloud fields, well-characterized estimates of tropospheric composition.

[46] Future work may include the study of the cloud properties that can be retrieved from TES data, implementation of cloud retrievals for limb viewing mode, and implementation of multiple layer clouds for nadir viewing mode.

Appendix A: Broken Clouds Can Be Handled With a Cloud-Effective Optical Depth

[47] When an atmosphere is otherwise homogeneous for each pressure layer in the 5 × 8 km air column observed by TES, a single-layer of broken clouds is mathematically equivalent to a uniform layer of less thick clouds. This allows the computation of a single radiative transfer rather than multiple radiative transfer calculations that are later averaged. This calculation is demonstrated using a radiative transfer through a three-layer atmosphere in Figure A1. The upwelling radiative transfer for the radiance observed above layer 3 is

$$\text{cloud free radiance} = \varepsilon B_{ground} T_1 T_2 T_3 + B_1(1 - T_1) T_2 T_3 + B_2(1 - T_2) T_3 + L_3$$

$$\text{cloudy radiance} = \varepsilon B_{ground} T_1 T_2' T_3 + B_1(1 - T_1) T_2' T_3 + B_2\left(1 - T_2'\right) T_3 + L_3$$

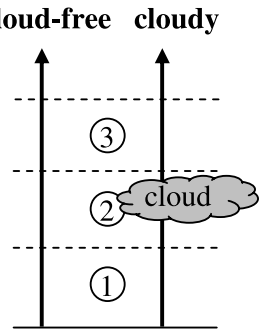

Figure A1. Diagram of radiative transfer through a three-layer atmosphere containing a nonuniform cloud. The right path goes through a cloud in layer 2, while the left path does not.

where T_2 is the transmission for the cloud-free layer 2, and T'_2 is the transmission for cloudy layer 2. If the layer 2 effective transmission is $T_{2,eff} = (aT_2' + (1 - a)T_2)$, where a and $(1 - a)$ are the fraction of the total radiance which comes from each path, then the total radiance is

$$\text{average radiance} = \varepsilon B_{ground} T_1 T_{2,eff} T_3 + B_1(1 - T_1)T_{2,eff} T_3 + B_2\left(1 - T_{2,eff}\right)T_3 + L_3$$

[48] From this equation, it can be seen that the inhomogeneity in any *one* layer can be mitigated by creating an "effective" transmission. This example can be expanded to include any number of cloud conditions in any *one* layer. The retrieved cloud extinction is then a combination of the cloud extinction for the cloud free and cloudy part of the field of view. The retrieved cloud extinction does not represent the cloud thickness at any location, but some average over the entire view. Note that inhomogeneity in more than one layer cannot be handled by this technique.

Appendix B: TES Cloud Jacobians

[49] Jacobians are the first derivatives of the radiation observed by TES ($\mathbf{L}$) with respect to retrieval parameters. Jacobians are used in the optimal estimation of the retrieval parameters (see equations (8) and (13)). This appendix briefly describes the equations used for the calculation of the Jacobians for cloud-effective extinction, κ_e ($\nu_\mathbf{c}$) and cloud height P_c. Descriptions of Jacobians for TES atmospheric profiles of temperature and trace gases can be seen in Clough et. al, 2005. Using the chain rule, and keeping in mind the equations describing the cloud optical depth, equations (1) to (4), the Jacobians for effective extinction, $\kappa_e(\nu_\mathbf{c})$ and cloud height P_c are

$$\frac{\partial \mathbf{L}(\boldsymbol{\nu}_{conv})}{\partial \ln(P_c)} = \frac{\partial \mathbf{L}(\boldsymbol{\nu}_{conv})}{\partial \boldsymbol{\tau}\left(\boldsymbol{\nu}_{conv}, \overline{\mathbf{P}}_l\right)} \frac{\partial \boldsymbol{\tau}\left(\boldsymbol{\nu}_{conv}, \overline{\mathbf{P}}_l\right)}{\partial \boldsymbol{\tau}\left(\boldsymbol{\nu}_c, \overline{\mathbf{P}}_l\right)} \frac{\partial \boldsymbol{\tau}\left(\boldsymbol{\nu}_c, \overline{\mathbf{P}}_l\right)}{\partial \ln(P_c)} \quad \text{(B1)}$$

and

$$\frac{\partial \mathbf{L}(\boldsymbol{\nu}_{conv})}{\partial \ln \boldsymbol{\kappa}(\boldsymbol{\nu}_c)} = \frac{\partial \mathbf{L}(\boldsymbol{\nu}_{conv})}{\partial \boldsymbol{\tau}\left(\boldsymbol{\nu}_{conv}, \overline{\mathbf{P}}_l\right)} \frac{\partial \boldsymbol{\tau}\left(\boldsymbol{\nu}_{conv}, \overline{\mathbf{P}}_l\right)}{\partial \boldsymbol{\tau}\left(\boldsymbol{\nu}_c, \overline{\mathbf{P}}_l\right)} \frac{\partial \boldsymbol{\tau}\left(\boldsymbol{\nu}_c, \overline{\mathbf{P}}_l\right)}{\partial \ln \boldsymbol{\kappa}(\boldsymbol{\nu}_c)} \quad \text{(B2)}$$

[50] The first two terms in equations (B1) and (B2) are the same in both equations. The first term is the same for clouds or atmospheric parameters, and can be calculated from equation (6). The second term is calculated from equations (2) and (3), where mapping is now from the convolved, rather than monochromatic, grid. The third term in both equations can be calculated using equation (1).

[51] **Acknowledgment.** This research was carried out at the Jet Propulsion Laboratory, California Institute of Technology, under a contract with the National Aeronautics and Space Administration.

References

Ackerman, S. A., C. C. Moeller, K. I. Strabala, H. E. Gerber, L. E. Gumley, W. P. Menzel, and S.-C. Tsay (1998), Retrieval of effective microphysical properties of clouds: A wave cloud case study, ***Geophys. Res. Lett.***, *25*, 1121–1124.

Aumann, H. H., et al. (2003), AIRS/AMSU/HSB on the Aqua mission: Design, science objectives, data products, and processing systems, *IEEE Trans. Geosci. Remote Sens.*, *41*(2), 253–264.

Beer, R. (2006), TES on the Aura mission: Scientific objectives, measurements, and analysis overview, *IEEE Trans. Geosci. Remote Sens.*, *44*(5), 1102–1105.

Bey, I., D. J. Jacob, R. M. Yantosca, J. A. Logan, B. D. Field, A. M. Fiore, Q. B. Li, H. Y. Liu, L. J. Mickley, and M. G. Schultz (2001), Global modeling of tropospheric chemistry with assimilated meteorology: Model description and evaluation, *J. Geophys. Res.*, *106*, 23,073–23,095.

Bloom, S., et al. (2005), Documentation and validation of the Goddard Earth Observing System (GEOS) data assimilation system, version 4, in *Technical Report Series on Global Modeling and Data Assimilation*, *NASA/TM-2005-104606*, *NASA Tech. Memo*, *26*. (Available at http://dao.gsfc.nasa.gov/pubs/docs/Bloom168.pdf)

Bowman, K. W., T. Steck, H. M. Worden, J. Worden, S. Clough, and C. Rodgers (2002), Capturing time and vertical variability of tropospheric ozone: A study using TES nadir retrievals, *J. Geophys. Res.*, *107*(D23), 4723, doi:10.1029/2002JD002150.

Bowman, K. W., et al. (2006), Tropospheric Emission Spectrometer: Retrieval method and error analysis, *IEEE Trans. Geosci. Remote Sens.*, *44*(5), 1297–1307.

Chahine, M. T. (1974), Remote sounding of cloudy atmospheres. 1. Single cloud layer, *J. Atmos. Sci.*, *31*, 233–243.

Chahine, M. T. (1977), Remote sounding of cloudy atmospheres. 2. Multiple cloud formations, *J. Atmos. Sci.*, *34*, 744–757.

Chahine, M. T., H. H. Aumann, and F. W. Taylor (1977), Remote sounding of cloudy atmospheres. 3. Experimental verifications, *J. Atmos. Sci.*, *34*, 758–765.

Clough, S. A., J. R. Worden, P. D. Brown, M. W. Shephard, C. P. Rinsland, and R. Beer (2002), Retrieval of tropospheric ozone from simulations of limb spectral radiances as observed from space, *J. Geophys. Res.*, *107*(D21), 4589, doi:10.1029/2001JD001307.

Clough, S. A., et al. (2006), Forward model and Jacobians for Tropospheric Emission Spectrometer retrievals, *IEEE Trans. Geosci. Remote Sens.*, *44*(5), 1308–1323.

King, M. D., Y. J. Kaufman, W. P. Menzel, and D. Tanre (1992), Remote-sensing of cloud, aerosol, and water-vapor properties from the Moderate Resolution Imaging Spectrometer (MODIS), *IEEE Trans. Geosci. Remote Sens.*, *30*, 2–27.

King, M. D., W. P. Menzel, Y. J. Kaufman, D. Tanre, B. C. Gao, S. Platnick, S. A. Ackerman, L. A. Remer, R. Pincus, and P. A. Hubanks (2003), Cloud and aerosol properties, precipitable water, and profiles of temperature and water vapor from MODIS, *IEEE Trans. Geosci. Remote Sens.*, *41*, 442–458.

McPeters, R. D., et al. (1998), Earth Probe Total Ozone Mapping Spectrometer (TOMS) Data Products User's Guide, *NASA Ref. Publ. 1998-206895*, NASA, Washington, D. C.

Menzel, W. P., W. L. Smith, and T. R. Stewart (1983), Improved cloud motion wind vector and altitude assignment using Vas, *J. Clim. Appl. Meteorol.*, *22*, 377–384.

Moncet, J. L., and S. A. Clough (1997), Accelerated monochromatic radiative transfer for scattering atmosphere: Application of a new model to spectral radiance observations, *J. Geophys. Res.*, *102*, 21,853–21,866.

Norton, R. H., and R. Beer (1976), New apodizing functions for Fourier spectrometry, *J. Opt. Soc. Am.*, *66*, 259–264.

Platnick, S., M. D. King, S. A. Ackerman, W. P. Menzel, B. A. Baum, J. C. Riedi, and R. A. Frey (2003), The MODIS cloud products: Algorithms and examples from Terra, *IEEE Trans. Geosci. Remote Sens.*, *41*, 459–473.

Rodgers, C. (2000), *Inverse Methods for Atmospheric Sounding: Theory and Practice*, World Sci., Hackensack, N. J.

Shephard, M. W., S. A. Clough, J. S. Delamere, K. Cady-Pereira, and E. J. Mlawer (2005), Validation of forward model with interferometric measurements for passive remote sensing, paper presented at the AFGL Transmission Meeting, 27th Annual Review of Atmospheric Transmission Models, IEEE, Lexington, Mass., 15–16 June.

Smith, W. L., H. M. Woolf, and W. J. Jacob (1970), A regression method for obtaining real-time temperature and geopotential height profiles from satellite spectrometer measurements and its application to Nimbus-3 Sirs observations, *Mon. Weather Rev.*, *98*, 582–603.

Susskind, J., C. D. Barnet, and J. M. Blaisdell (2003), Retrieval of atmospheric and surface parameters from AIRS/AMSU/HSB data in the presence of clouds, *IEEE Trans. Geosci. Remote Sens.*, *41*, 390–409.

Wei, H. L., P. Yang, J. Li, B. A. Baum, H. L. Huang, S. Platnick, Y. X. Hu, and L. Strow (2004), Retrieval of semitransparent ice cloud optical thickness from atmospheric infrared sounder (AIRS) measurements, *IEEE Trans. Geosci. Remote Sens.*, *42*(10), 2254–2267.

Worden, J., S. S. Kulawik, M. W. Shephard, S. A. Clough, H. Worden, K. Bowman, and A. Goldman (2004), Predicted errors of Tropospheric Emission Spectrometer nadir retrievals from spectral window selection.

R. Beer, K. Bowman, A. Eldering, M. Gunson, S. S. Kulawik, G. Osterman, and J. Worden, Jet Propulsion Laboratory/California Institute of Technology, 4800 Oak Grove Drive, Pasadena, CA 91109, USA. (susan.s.kulawik@jpl.nasa.gov)

S. A. Clough and M. Shephard, Atmospheric and Environmental Research Inc. (AER), 131 Hartwell Avenue, Lexington, MA 02421, USA.

L. Zhang, Department of Earth and Planetary Sciences, Harvard University, Cambridge, MA 02138, USA.